

Bi-Modal Hemispherical Sensor: A Unifying Solution for Three Axis Force and Contact Angle Measurement

Meng Yee (Michael) Chuah^{1,*}, Lindsay Epstein^{2,*}, Donghyun Kim², Juan Romero², and Sangbae Kim²

Abstract—In robotic tasks that require physical interactions such as manipulation and legged locomotion, it is important to simultaneously measure contact forces and contact angles. This paper presents a unified solution for simultaneously measuring three axis contact forces and contact angles for legged locomotion or manipulation. Unlike most tactile sensors, the presented design utilizes the stress field method by sampling pressures over multiple locations within an elastomer, enabling inherently robust operation against impact and abrasive interactions. The presented sensor is designed for point-feet quadrupedal robots and can be easily scaled down for other applications such as grasping. The sampled stress distribution is mapped to output forces f_x , f_y , and f_z and two contact angles, θ and ϕ on the hemispherical sensor surface via Gaussian process regression. The prototype sensor is able track normal and shear forces accurately, achieving a normalized root mean (RMS) squared error of only 1.00% – 1.36% for f_z across multiple tests with up to 180N normal force, and a normalized RMS error of 1.71% – 4.67% and 1.82% – 6.68% for f_x and f_y , respectively, with up to 80N shear force. Additionally, the footpad is able to estimate the contact location coordinates θ and ϕ with a normalized RMS error of 2.69% – 7.51% over a range of 0 – 40° and 2.79% – 9.62% over a range of 0 – 30°, respectively. The footpad can estimate contact location over a maximum range of $\theta = \pm 45^\circ$ and $\phi = \pm 45^\circ$, and can withstand over 450N of normal force at location $\theta = \phi = 0^\circ$ without reaching saturation. This prototype demonstrates the ability to simultaneously measure force in three axes and contact angles using Gaussian process regression, with the potential to explore other regression methods for embedded computing and miniaturization of the design for finger tip scale sensors.

I. INTRODUCTION

Fast and robust contact sensing for dynamic physical interactions is a crucial step in developing high performance robots in the future. Although most factory robots successfully operate primarily on position commands without relying on tactile cues, many future robotic applications will require rich sensing for faster and more robust operation. The ability to swiftly manipulate a variety of objects or complete agile legged locomotion in an unstructured environment requires quick sensing of contact forces and contact surface angles [1]. In the area of manipulation, more stable grasping can be achieved if contact forces and the surface normal of the contact is measured by the robotic finger as soon as it touches the object. In locomotion, legged robots can be more

agile if given the ability to accurately and simultaneously sense both the ground reaction forces and angle, which can provide early detection of slip or a better estimation of the friction cone based on the surface normal. In many robotic applications with physical interactions, measurement of the contact forces and the contact angle can provide crucial information for faster, more stable, and more resilient operations. Despite this, many existing sensors fail to provide the necessary information or cannot withstand dynamic, high force use.

Conventional strain gauge based force-torque sensors used in robotics have limited utility for physical interactions that require fast contact or impact. Typical multi-axis force sensors made of high stiffness materials relate the linear strain of the structure to the output force or torque. While these types of sensors are very accurate and repeatable, they can cause several problems when used for dynamic physical interactions. First, these sensors are fragile upon impact due to their high stiffness. Second, these sensors are inherently sensitive to inertial noise due to their design topology. Third, the sensors tend to be heavy and expensive. In order to reliably provide contact information in dynamic legged robots and rapid manipulation we need different types of sensors that are lighter, softer, cheaper and more robust against impacts and abrasion.

Other sensing options include tactile sensing techniques which are commonly used in contact location detection. Typically, these sensors take the form of a thin sheet containing an array of sensors that detect pressure [2], [3] or electric capacitance [4]. While these sensors are good at detecting contact location in lower force applications, they are not suitable for multi-axis force measurement in robotic finger tips or on the feet of legged robots, especially when these robots are performing dynamic tasks.

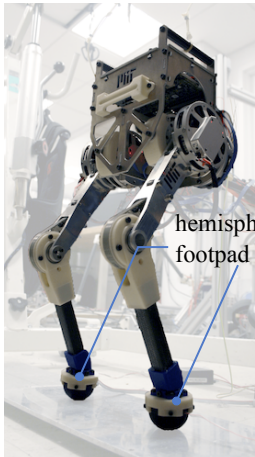
A number of other sensors have also been developed, many of which are intended for use in robotic grippers. These include magnetic Hall-Effect based sensors [5], [6], the GelSight tactile sensor [7], the SynTouch BioTac sensor [8], tactile sensing arrays [2] and other rubber embedded stress field based sensors [3], [9].

Among these newly developed sensing mechanisms, Gel-sight [7], [10] provides extremely rich information including contact force estimation and details about the contact surface structure. It does this by measuring the deformation of an elastomer using multiple cameras and 3D reconstruction. This rich information has extended the capabilities of robotic manipulators, allowing them to estimate the quality of their grasps [10]. With a smaller form factor and faster image

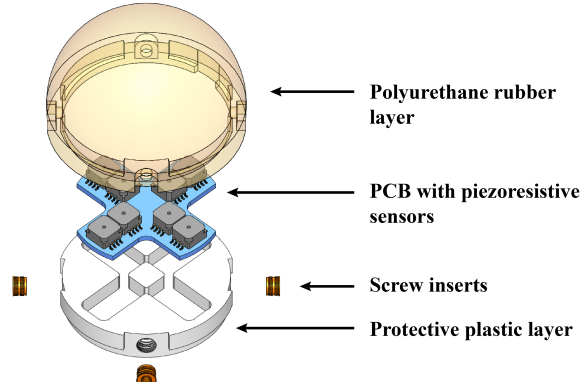
*These authors contributed equally to this work

¹Author is with the Robotics and Autonomous Systems (RAS) department of the Institute for Infocomm Research (I2R), part of the Agency for Science, Technology and Research (A*STAR) in Singapore. mcccxxx@gmail.com or michael_chuah@i2r.a-star.edu.sg

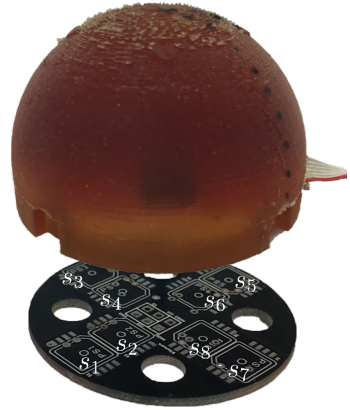
²Authors are with the Biomimetic Robotics Laboratory at the Department of Mechanical Engineering, Massachusetts Institute of Technology (MIT), Cambridge, MA, 02139, USA. lepstein@mit.edu



(a) Little HERMES robot



(b) Exploded view of the hemispherical footpad



(c) Sensor and PCB

Fig. 1. Reliable force and contact location footpad sensor development for dynamic legged robots. (a) Little HERMES is a bipedal robot developed to study teleoperation and human in the loop control. Here it has been outfitted with hemispherical footpads capable of measuring normal and shear forces, as well as contact location. (b) Exploded view of the hemispherical footpad showing piezoresistive sensor locations. The sensors and PCB are embedded in the translucent polyurethane rubber material as labeled in the figure. (c) Completed hemisphere footpad. The eight pressure sensors are located on the PCB as indicated.

processing Gelsight also has the potential to be used in many other applications. This represents a step in the direction of more robust contact sensing for dynamic applications.

Chuah [11]–[13] developed a lightweight, robust, low cost force sensing footpad with low inertial noise using a stress field sensing method. In this sensor, the contact forces are inferred from the stress distribution in an elastomeric footpad, which allows for shielding from most inertial noise. This approach allows for robust, cheap, fast three axis sensing for flat-to-flat contact situations, but cannot provide contact location or contact angle. In reality, gripper fingers and legged robot feet often experience quasi point contact with changing contact angles. Therefore, in order to properly infer the contact details and more accurately estimate the allowable contact force range for secure contact, contact sensors should provide contact force and contact angle measurements simultaneously.

This paper presents a unified solution for measuring three axis contact forces and contact angle for quasi point contact situations such as hemispherical finger tip or round feet contact with ground. This new sensor design utilizes piezoresistive barometers to sample the stress field within an elastomeric hemisphere, then employs Gaussian process regression to infer both contact angle and the contact forces in three axes. The sensor is unique in its low cost, robust design, and ability to measure both contact location and forces simultaneously.

The paper is structured as follows. Section II will discuss the design and fabrication of the hemispherical footpad. Section III will detail the experimental setup used to collect both the training data set and the validation data set. Section IV will talk about the process of elucidating the normal and shear force estimators along with the contact location estimator from the piezoresistive sensor signals in the hemispherical footpad using Gaussian process regression. Section V will

present the experimental results of further testing of the hemispherical footpads including roll, manual manipulation, and impact testing. Section VI will then outline potential improvements to the hemispherical footpad prototypes that are the subject of both ongoing and future works.

II. HEMISPHERICAL FOOTPAD DESIGN AND FABRICATION

The hemispherical footpad prototype as seen in Fig. 1(b) incorporates improvements and design variations from the previous design described by Chuah et al. [11]–[13] in which the goal is to build a lightweight, low cost, yet robust footpad sensor suitable for use in legged robots undergoing ground locomotion. The design changes resulting in the hemispherical footpad were made to allow for improved shear sensitivity, contact detection, and ground contact location detection.

Eight barometric pressure sensors (MPXH6400A from Freescale Semiconductor) are modified to act as piezoresistive sensors using the procedures outlined in [11]–[13]. An array of eight pressure sensors was chosen, as opposed to previous designs which included four or six pressure sensors, in order to better decouple x and y shear force from contact location estimation while maintaining sensor symmetry. These piezoresistive sensors are then soldered onto a circular printed circuit board (PCB) of 43mm diameter and numbered clockwise from outside to inside (Fig. 1(c)). The minimum size of the PCB is limited by the size of the pressure sensors, which were chosen for their specific pressure range (20–400kPa), footprint, calibration, and temperature compensation. For future work, smaller pressure sensors are being investigated that would allow the overall size of the PCB, and the footpad sensor, to decrease. For other applications in which the observed forces are lower and a smaller size is desirable, such as in robotic grippers,

pressure sensors with a lower maximum pressure and smaller footprint could also be used.

The sensing elements, which include the PCB and associated electronics, are embedded within a hard plastic layer, which also holds the screw inserts in place. This plastic layer with embedded PCB is then over-molded with a hemisphere of translucent polyurethane rubber of Shore A hardness 20 (Vytaflex 20 from Smooth-On). To form the hemisphere, uncured polyurethane rubber is poured into a 3D printed mold containing the hard plastic layer with exposed piezoresistive sensors. This mold is then placed in a vacuum chamber to remove any air bubbles trapped between the polyurethane rubber and the piezoresistive sensors. After curing for 16 hours the liquid polyurethane rubber solidifies, resulting in a completely monolithic footpad that is totally isolated from the external environment, making it robust and waterproof. The key differences between this design and previous iterations are the shape of the polyurethane rubber layer and the number of pressure sensors on the PCB. All of this can be seen in Fig. 1(b). The final footpad sensor is a hemisphere with a diameter of 56mm.

When the rubber of the footpad contacts the ground and undergoes deformation, the stress field within the hemispherical footpad changes. How it varies is determined by the x , y , and z forces, as well as the location of the point at which the hemisphere contacts the ground (determined by angles θ , measured about the x axis, and ϕ , measured about the y axis, as seen in Fig. 4. This unique change in stress field results in a change in the analog signals output by the piezoresistive sensor array. These analog signals are passed through an on-board 12-bit Analog-to-Digital Converter (ADC) (MCP3208 from Microchip Technology), then sent to a microcontroller, and finally used to reconstruct the ground interaction forces and contact locations.

III. EXPERIMENTAL SETUP FOR DATA COLLECTION

To collect data from the footpad sensor that can be correlated with known force and ground contact angle readings, a modified 3-axis CNC milling machine (MicroMill DLS 3000 from MicroProto Systems), a 6-axis force/torque sensor (ATI Delta SI-660-60 from ATI Industrial Automation) and a rotary magnetic encoder (AEAT-6012 from Avago Technologies) were used. The force/torque sensor and rotary magnetic encoder were used as the ground truth, while the CNC milling machine was programmed to act as a positioner to bring the footpad sensor into contact with the force/torque sensor and move it through a set trajectory. To allow the hemisphere to make contact at various points across its surface, the 3-axis CNC milling machine was altered to include mounting features for the footpad sensors and to incorporate a fourth rotary with a trunnion table to perform roll about the x axis of the mill. A manual rotation stage (2" Manual Rotation Stage RP01/M from Thor Labs) was also added to the CNC mill in order to rotate the footpad about the z axis of the mill. This is largely the same procedure used previously in [11]–[13], with the key difference from previous works being that normal and shear data sets can now

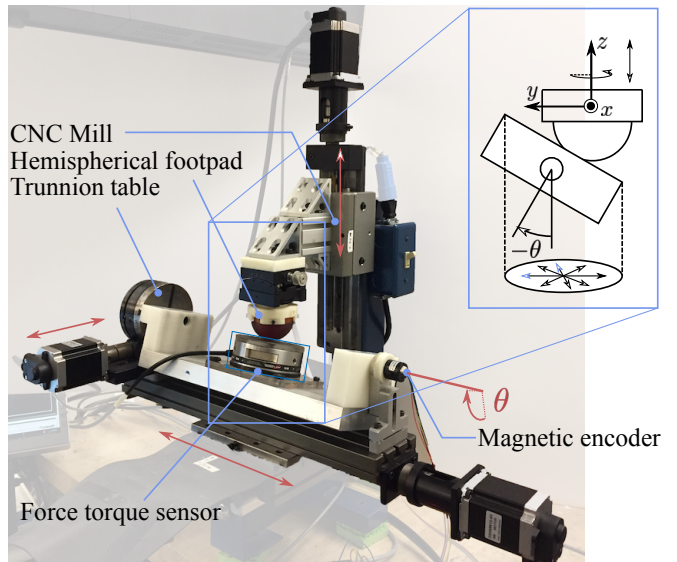


Fig. 2. **Experimental setup.** The footpad sensor is mounted to the CNC spindle mount and brought into contact with the force/torque sensor. A prescribed trajectory is then assigned, and data is collected using NI LabVIEW.

be collected at different contact locations on the surface of the hemisphere. Fig. 2 shows the experimental setup with the CNC mill pressing the footpad sensor onto the force/torque sensor.

Data was collected for contact points across $1/8^{th}$ of the hemisphere surface using rotation about the x axis from 0° to 40° spaced at 10° increments, and rotation about the z axis from 0° to 45° spaced at 15° increments. This corresponds to contact locations in the range $\theta = 0^\circ$ to $\theta = 45^\circ$ and $\phi = 0^\circ$ to $\phi = 30.68^\circ$ where θ and ϕ are sequential explicit rotations about x and y axis, respectively, as seen in Fig. 4. Forces are defined in the sensor coordinate systems such that f_x and f_y are tangent to the rubber hemisphere surface (shear forces) and f_z is normal to the rubber hemisphere surface (normal force).

At each contact location, the sensor was moved through an asterisk shaped path normal to the surface of the ATI force/torque sensor at various levels of compression (Fig. 3). This data was then separated into two groups - data to be used for training and data to be used for testing or validation. While the data shown in this paper primarily focuses on contact points covering $1/8^{th}$ of the hemisphere surface, the results are expected to be applicable to the whole hemispherical surface due to the symmetry of the sensor. To validate this assumption, data was later collected for points covering the entire hemispherical surface, as will be discussed in Section VI.

As the footpad sensor moves through each trajectory, 12-bit analog values from the piezoresistive sensors embedded in the hemispherical footpad and from the rotary encoder are read via SPI by a NUCLEO-L432KC microcontroller at a 1kHz sampling rate. Concurrently, the normal and shear force readings from the force/torque sensor are collected through a data acquisition system (CompactDAQ 9205 from

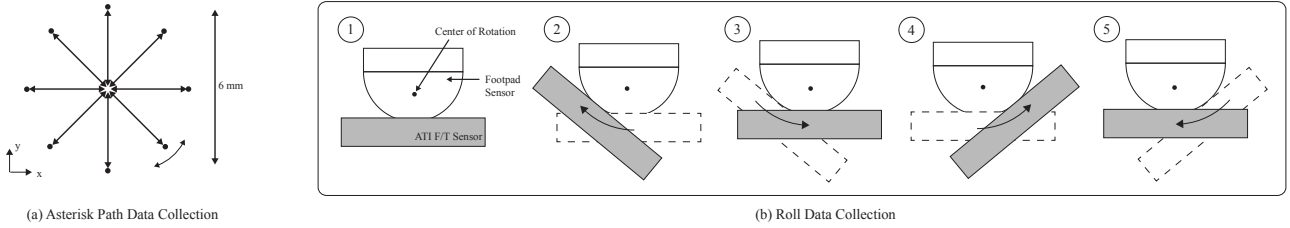


Fig. 3. **Data Collection Setup.** (a) To obtain initial training and validation data the footpad was brought into contact with the force/torque sensor at different contact locations and moved through the asterisk shaped path shown. (b) To simulate rolling contact the trunnion table of the mill was used to rotate the force/torque sensor about the surface of the footpad.

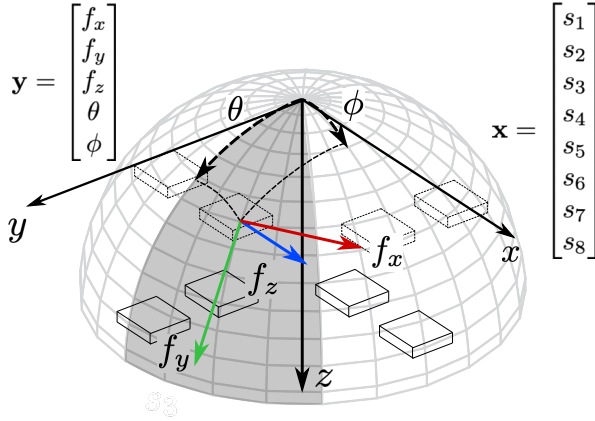


Fig. 4. **Sensor configuration.** The estimated contact force is presented in the local frame, of which the z axis is orthogonal to the contact surface. Contact location is described by sequential rotation θ and ϕ , which are rotations about x and y axis, respectively. Shaded region indicates the portion of the hemispherical surface over which the sensor was trained and tested.

National Instruments (NI)), also at 1kHz. The voltages from the footpad and encoder and the forces from the force/torque sensor are all synchronized in NI LabVIEW before being exported as data sets for further processing in MATLAB.

IV. FORCE AND ANGLE ESTIMATION

A. Gaussian Process Regression

The relationship between the eight pressure sensor readings and the contact force and angle is too complex to be analytically modeled. Instead, Gaussian process regression (GPR) [14] is utilized to find the mapping between sensor signals and output signals and provide reliable force and angle estimation. Fig. 4 summarizes the input and output data used in the estimation. The input vector, \mathbf{x} , is composed of the voltage signals from the eight pressure sensors, $[s_1, s_2, \dots, s_8]^\top$. The output vector, \mathbf{y} , consists of the contact location, described by angles θ and ϕ , and the linear force at that location, $[f_x, f_y, f_z]^\top$. The GPR is first trained using a training data set, then evaluated using a validation data set.

Using GPR, an estimation of the scalar output \hat{y}_j (i.e. estimated f_x, f_y, f_z, θ , or ϕ) for any new vector input \mathbf{x}_* (i.e. $[s_1, s_2, \dots, s_8]^\top$) can be calculated using the equation:

$$\hat{y}_j = \mathbf{k}_* (\mathbf{K} - \sigma_n \mathbf{I})^{-1} \mathbf{y}_j, \quad (1)$$

where \mathbf{y}_j is a $n \times 1$ vector consisting of the measured value of the output being estimated for each point in the training data set of n points, \mathbf{K} is the covariance matrix, and σ_n is the standard deviation. The training data set has $n = 5,649$ points. Because \hat{y} is a scalar output, the computation in Eq. (1) must be completed five times on each input \mathbf{x}_* in order to provide a full output estimation vector \mathbf{y} including f_x, f_y, f_z, θ , and ϕ . \mathbf{k}_* and \mathbf{K} are calculated as follows:

$$\mathbf{k}_* = [k(\mathbf{x}_*, \mathbf{x}_1) \quad k(\mathbf{x}_*, \mathbf{x}_2) \quad \dots \quad k(\mathbf{x}_*, \mathbf{x}_n)], \quad (2)$$

$$\mathbf{K} = \begin{bmatrix} k(\mathbf{x}_1, \mathbf{x}_1) & k(\mathbf{x}_1, \mathbf{x}_2) & \dots & k(\mathbf{x}_1, \mathbf{x}_n) \\ \vdots & \ddots & & \vdots \\ k(\mathbf{x}_n, \mathbf{x}_1) & \dots & k(\mathbf{x}_n, \mathbf{x}_n) \end{bmatrix}. \quad (3)$$

Note that all terms in Eq. (1) except \mathbf{k}_* are independent of the new input \mathbf{x}_* . This means that although the computation of $(\mathbf{K} - \sigma_n \mathbf{I})^{-1} \mathbf{y}_j$ requires high computational effort due to the matrix inversion, a complete estimation given new input data \mathbf{x}_* takes less than 1ms after the system has been trained. On a Ryzen Threadripper 1950X 4GHz CPU the average computation time of the estimation is 0.3 ms.

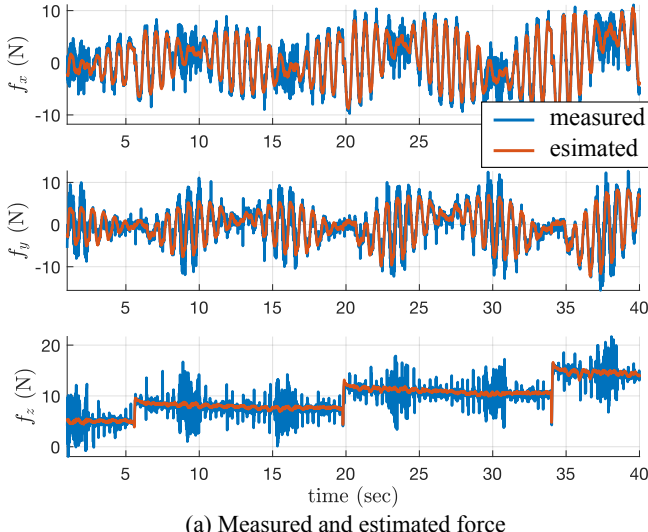
When calculating \mathbf{K} , a squared-exponential covariance function was used as the kernel k :

$$k(\mathbf{x}_1, \mathbf{x}_2) = \sigma_f^2 \exp\left(-\frac{1}{2l^2} \|\mathbf{x}_1 - \mathbf{x}_2\|^2\right), \quad (4)$$

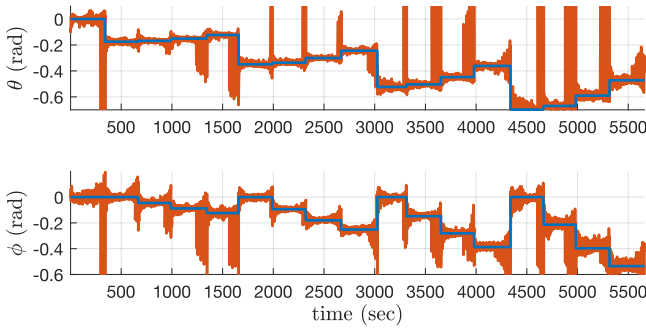
where σ_f and l represent signal variance and length-scale. The hyperparameters, σ_n , σ_f , and l were manually tuned by evaluating the result of the regression using the validation data set.

B. Regression Results

After the footpad and reference data were collected for multiple contact locations and compression amounts, as discussed above, this data was divided into a training data set and a validation data set. 1 out of every 1000 data points was used for the training data set, while 1 out of every 10 data points was used for the validation data set. The training data set was used to train GPR, while validation data set was used to validate the fit. The root mean squared (RMS) error and coefficient of determination R^2 between the Gaussian



(a) Measured and estimated force



(b) Contact orientation estimation

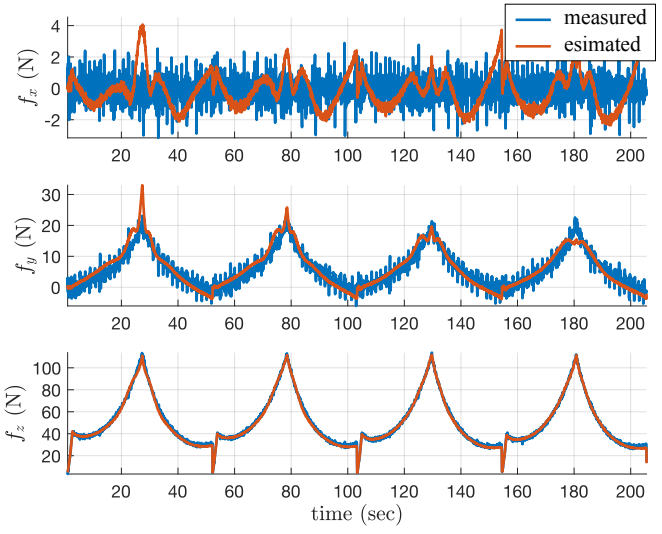
Fig. 5. Regression result. (a) Contact force estimation shows a good agreement between measured and estimated forces. Only a portion of the data is shown for clarity. (b) Contact angles for multiple trials are plotted. The estimation data displays a spike when the contact angles is changed between trials as the sensor is no longer in contact with the ground.

process force estimators and the measured forces for the validation data set are shown in Table I as a way to evaluate the goodness of fit of the estimator.

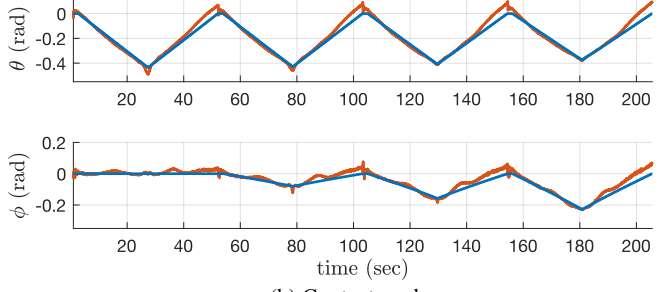
Fig. 5 and Table I both show that there is a good agreement between the estimated and measured forces and angles. The large spikes observed in the contact location estimate correspond to times when f_z of the sensor is very low or 0. This occurs when the sensor is barely, or not at all in contact with the ground, and therefore cannot estimate contact angle. These spikes were included in all RMS error and R^2 calculations, however they make up a very small portion of the data and therefore did not significantly impact performance. When compared to other force sensors based on silicon pressure sensors, the footpad force estimation performs favorably. De Rossi et al. have created force sensors for use in a physical human-robot interface of a lower-limb exoskeleton, and they obtain normalized RMS errors that range from 2.7% to 8.5% for their normal force estimation [15].

TABLE I
RMS ERROR, NORMALIZED RMS ERROR, AND R^2
VALIDATION DATA

	RMS Error (N)	Norm. RMS Error (%)	R^2 (%)
f_x	1.537	1.709	98.126
f_y	2.259	1.824	96.491
f_z	1.870	1.001	99.704
θ	0.019	2.689	99.065
ϕ	0.0149	2.790	99.123



(a) Contact force



(b) Contact angle

Fig. 6. Rolling test results. Footpad estimations and measured sensor readings for f_x , f_y , f_z , θ , and ϕ .

$$RMS\ Error = \left[\frac{1}{n} \sum_{i=1}^n (\hat{y}_i - y_i)^2 \right]^{\frac{1}{2}}, \quad (5)$$

$$R^2 = \left[1 - \frac{\sum_{i=1}^n (y_i - \bar{y})^2}{\sum_{i=1}^n (y_i - \hat{y}_i)^2} \right] \times 100\%, \quad (6)$$

V. EXPERIMENTAL VALIDATION

To further validate the footpad performance, two additional sets of tests were performed. These tests were intended to more accurately reflect the potential types of motion the footpad might experience while in use on a robot.

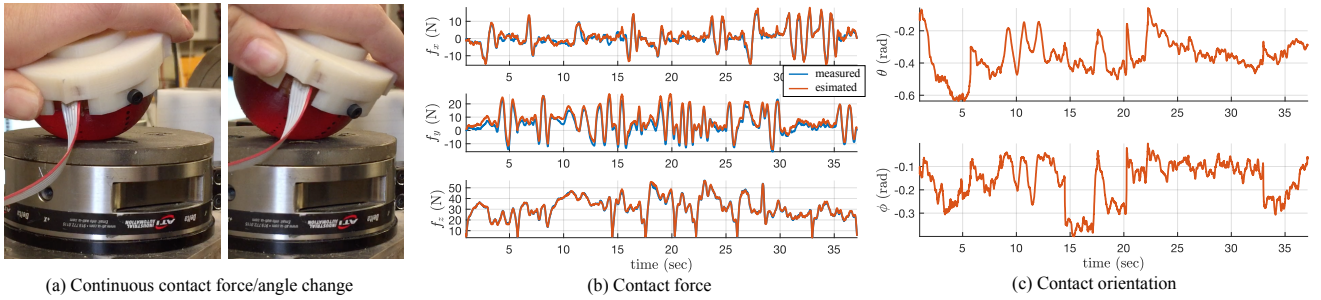


Fig. 7. **Manual force test.** (a) Image showing how the test was conducted, as can also be seen in attached video. (b) Estimated and measured f_x , f_y , and f_z forces. (c) Estimated contact location θ and ϕ . No ground truth contact location data was recorded for hand manipulation trials.

TABLE II
RMS ERROR, NORMALIZED RMS ERROR, AND R^2
ROLL DATA

	RMS Error (N)	Norm. RMS Error (%)	R^2 (%)
f_x	1.424	22.226	-219.569
f_y	2.300	6.685	84.445
f_z	1.474	1.327	99.587
θ	0.033	7.509	92.936
ϕ	0.022	9.617	85.876

TABLE III
RMS ERROR, NORMALIZED RMS ERROR, AND R^2
HANDHELD DATA

	RMS Error (N)	Norm. RMS Error (%)	R^2 (%)
f_x	1.450	4.674	92.609
f_y	2.5597	6.167	90.618
f_z	0.725	1.365	99.454

A. Roll Data

The first set of additional tests are intended to reflect the “rolling” contact the footpad may experience during walking, and to test the ability of the sensor to determine contact location while experiencing both normal and shear forces. This test consisted of compressing the footpad a set amount (2 mm), then using the trunnion table of the CNC mill to roll along the footpad surface between 0° and 25° at a fixed rotation about the z axis (Fig. 3). This was repeated for z axis rotations of $0^\circ, 10^\circ, 20^\circ$, and 30° . Fig. 6 and Table II both show that there is generally a good agreement between the measured and estimated forces and angles. One exception to this is the f_x data. This is due to the very low (≈ 0 N) f_x observed during trials in which the mill was rolling about the x axis. The magnitude of the estimated f_x is comparable to the magnitude of noise in the force/torque sensor data. The lower R^2 value for the f_y data is also likely due to a large amount of noise in the force/torque sensor data, relative to the measured f_y .

B. Manual Force Data

The second set of additional tests were collected by manually manipulating the footpad sensor through a range of different motions against the surface of the ATI force/torque sensor to create a random input of contact locations, shear, and normal forces over time. The contact locations tested were intentionally kept within or near the $1/8^{th}$ hemisphere surface on which the system had been previously trained. Fig. 7 and Table III show that there is a good agreement between the estimated and measured forces. At very low forces (< 2 N) some offset was observed between the measured and

estimated tangential force. This is likely due to omission of data from the training dataset in which the sensor was not at all or barely making contact with the force/torque sensor, defined as having a norm of all pressure sensor outputs below 60 mV (≈ 5 N). The quality of the angular estimation could not be quantified as there is no reference contact location for comparison in the handheld tests. In future work a motion capture system or IMU will be used to quantify the performance of the angular estimation during handheld data collection. Due to the accuracy limits of manual human positioning, there may have been a small mismatch between the coordinate frames of the footpad and the ATI F/T sensor.

C. Impact Resistance Test

To give a qualitative measure of the durability of the sensor, impact and high force compression tests were also conducted. For the impact test, the footpad sensor was first manually compressed to demonstrate normal sensor functionality. The footpad sensor was then struck repeatedly with a hammer, causing the individual pressure sensor readings to saturate. Following this, the footpad sensor was tested again to ensure that it was still functioning. Results can be seen in Fig. 8. In the compression test, the sensor was compressed on the mill at a contact location of $\theta = 0^\circ$ and $\phi = 0^\circ$ to a force of above 450N without saturating (Fig. 9).

The effect of gravity due to changes in footpad orientation were also quantified. Gravitational effects were found to be negligible at 0.17% of the sensor reading at full scale which corresponds a deviation of less than 1N.

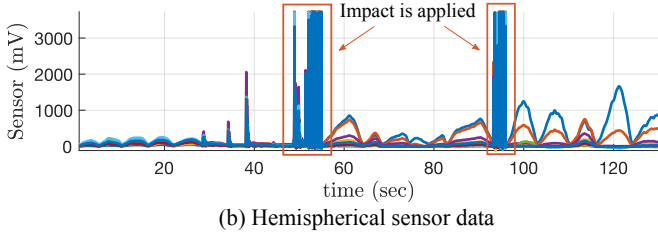
VI. DISCUSSION AND CONCLUSION

A. Discussion and Future Works

This hemispherical footpad sensor demonstrates the ability to decouple shear and normal forces, determine contact



(a) Normal operation test after impact



(b) Hemispherical sensor data

Fig. 8. (a) Footpad sensor undergoing impact testing. Footpad was struck with a hammer multiple times and then pushed by hand to confirm normal sensor operation. (b) Output of the footpad sensor before, during, and after high impact. Sensor saturation is visible in the pressure sensor data during impact. Even after high impacts, the sensor functions normally.

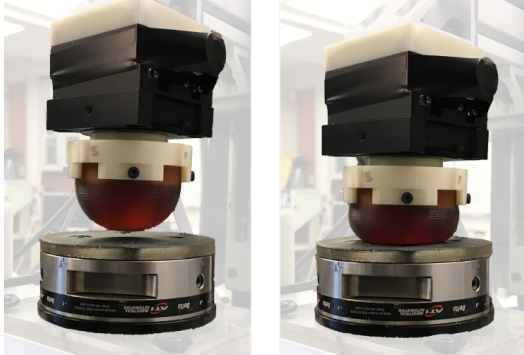
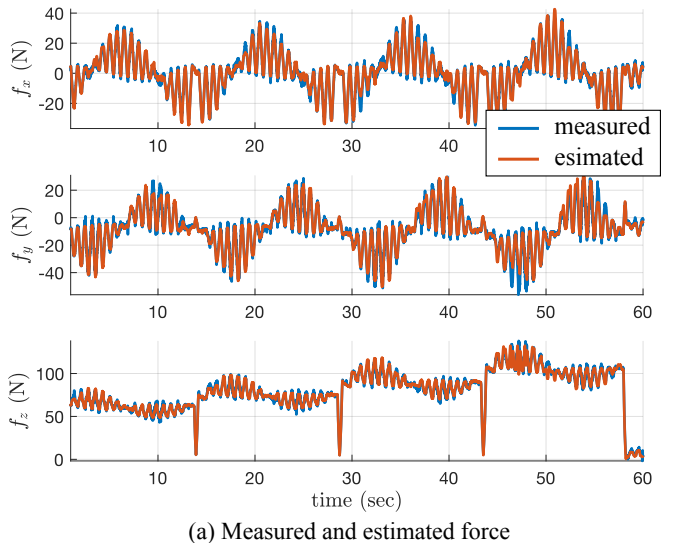


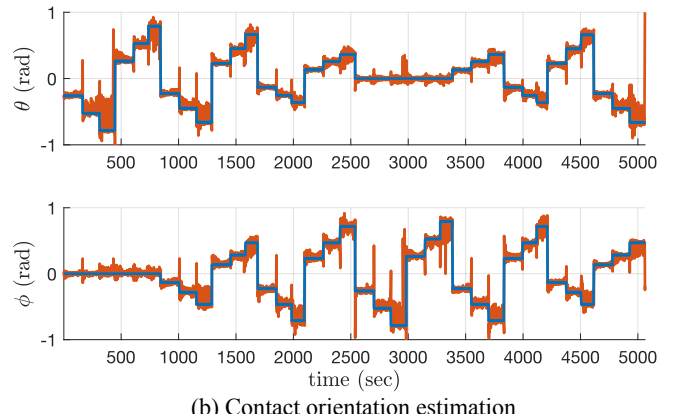
Fig. 9. Maximum compression test. The footpad sensor was compressed with up to 450N of force without reaching saturation.

location, and withstand high impacts. The sensor is also low cost, waterproof, and well suited for integration onto point feet quadrupedal robots.

While the results in this paper focus on data collected over $1/8^{th}$ of the hemispherical surface, additional data was collected to demonstrate the potential for this method to extend to cover the entire hemispherical surface. Using the same data collection process as before, data was collected for contact points across the full hemispherical surface using rotation about the x axis from -45° to 45° spaced at 15° increments, and rotation about the z axis from 0° to 180° spaced at 30° increments. At each contact location, the sensor was moved through an asterisk shaped path normal to the surface of the force/torque sensor at various levels of compression. This data was used to train and validate a new



(a) Measured and estimated force



(b) Contact orientation estimation

Fig. 10. Full hemisphere test. (a) Contact force estimation shows a good agreement between measured and estimated forces. Only a portion of the data is shown for clarity. (b) Contact angles for multiple trials covering points across the full surface of the hemisphere are plotted.

Gaussian process regression model. Results can be seen in Fig. 10.

Future testing will involve further analyzing data that covers the entire surface of the hemisphere and implementing and testing the sensor on the MIT Cheetah [11]–[13], [16] or the Little HERMES bipedal robot [17], [18] to further evaluate performance.

Future work will also focus on optimizing the design and fabrication of the sensor itself. The current process for making the footpad sensor has not been optimized for repeatability or manufacturing, with some variability between sensors arising due to fabrication (i.e. hand soldering of components resulting in slight changes to the piezoresistive sensor positions, or trapped bubbles during the degassing step). By eliminating these variations, it may be possible to use the same trained Gaussian process regression model on multiple footpad sensors. Investigating other materials with a more linear response may also help improve the performance of the sensor. Chuah's thesis [19] includes an analysis of the hysteresis of the polyurethane material currently used in the footpad sensor.

Natural extensions to this sensor design include miniaturization of the sensor for use in other applications such as providing accurate force and contact angle estimations in robotic manipulation. This design can be easily scaled by selecting pressure sensors with the correct size and pressure range for the desired application.

B. Conclusion

This paper presents a hemispherical footpad intended for use in robots undergoing legged locomotion that is able to accurately measure both the normal and shear ground reaction forces, as well as the ground contact location. The hemispherical footpad is able to achieve a normalized RMS error of only 1.00% – 1.36% for f_z across multiple tests with up to 180N normal force, and an average normalized RMS error of 1.71% – 4.67% and 1.82% – 6.68% for f_x and f_y , respectively, with up to 80N shear force. It can also predict the contact location coordinates θ and ϕ with a normalized RMS error of 2.69% – 7.51% over a range of 0 – 40° and 2.79% – 9.62% over a range of 0 – 30°, respectively. The range of angles over which the footpad can detect contact location is described by $\theta = \pm 45^\circ$ and $\phi = \pm 45^\circ$. The maximum compressive force that the footpad can experience without saturating is above 450N, and the footpad can withstand high force impacts without damage.

This type of hemispherical footpad sensor is lightweight, impact-robust, and suitable for use in legged robots undergoing dynamic locomotion. It would greatly aid legged robots in generating good state estimations, thereby enabling these robots to perform dynamic movements over uneven terrain. Beyond legged locomotion, this concept can be easily extended to other robotic applications such as dexterous manipulation. This sensor presents a viable option for fast and robust contact angle and force sensing for dynamic physical robotic interactions.

ACKNOWLEDGMENTS

The authors would like to thank Albert Wang and Joao Ramos of the MIT Biomimetic Robotics Laboratory for their invaluable assistance in this work.

REFERENCES

- [1] A. Seyfarth, H. Geyer, M. Günther, and R. Blickhan, “A movement criterion for running,” *J. Biomech.*, vol. 35, no. 5, pp. 649–655, 2002.
- [2] Y. Tenzer, L. P. Jentoft, and R. D. Howe, “The feel of mems barometers: Inexpensive and easily customized tactile array sensors,” *IEEE Robotics Automation Magazine*, vol. 21, no. 3, pp. 89–95, Sep. 2014.
- [3] J. W. Guggenheim, L. P. Jentoft, Y. Tenzer, and R. D. Howe, “Robust and inexpensive six-axis forcetorque sensors using mems barometers,” *IEEE/ASME Transactions on Mechatronics*, vol. 22, no. 2, pp. 838–844, April 2017.
- [4] X. A. Wu, T. M. Huh, R. Mukherjee, and M. Cutkosky, “Integrated ground reaction force sensing and terrain classification for small legged robots,” *IEEE Robotics and Automation Letters*, vol. 1, no. 2, pp. 1125–1132, July 2016.
- [5] T. P. Tomo, S. Somlor, A. Schmitz, L. Jamone, W. Huang, H. Kristanto, and S. Sugano, “Design and characterization of a three-axis hall effect-based soft skin sensor,” *Sensors*, vol. 16, no. 4, 2016.
- [6] D. S. Chathuranga, Z. Wang, Y. Noh, T. Nanayakkara, and S. Hirai, “Magnetic and mechanical modeling of a soft three-axis force sensor,” *IEEE Sensors Journal*, vol. 16, no. 13, pp. 5298–5307, July 2016.
- [7] W. Yuan, S. Dong, and E. H. Adelson, “Gelsight: High-resolution robot tactile sensors for estimating geometry and force,” *Sensors*, vol. 17, no. 12, 2017.
- [8] N. Wettsels and G. E. Loeb, “Haptic feature extraction from a biomimetic tactile sensor: Force, contact location and curvature,” in *2011 IEEE International Conference on Robotics and Biomimetics*, Dec 2011, pp. 2471–2478.
- [9] C. Reeks, M. G. Carmichael, , and K. J. Waldron, “Angled sensor configuration capable of measuring tri-axial forces for phri,” in *2016 IEEE International Conference on Robotics and Automation (ICRA)*, May 2016, pp. 3089–3094.
- [10] S. D. D. Ma*, E. Donlon* and A. Rodriguez, “Dense tactile force distribution estimation using gelslim and inverse fem,” in *ICRA*, 2019.
- [11] M. Y. M. Chuah, M. Estrada, and S. Kim, “Composite Force Sensing Foot Utilizing Volumetric Displacement of a Hyperelastic Polymer,” in *IEEE/RSJ International Conference on Intelligent Robots and Systems*, 2012, p. 67.
- [12] M. Y. M. Chuah and S. Kim, “Enabling Force Sensing During Ground Locomotion: A Bio-Inspired, Multi-Axis, Composite Force Sensor Using Discrete Pressure Mapping,” *IEEE Sensors Journal*, vol. 14, no. 5, pp. 1693–1703, May 2014.
- [13] M. Y. M. Chuah and S. Kim, “Improved normal and shear tactile force sensor performance via Least Squares Artificial Neural Network (LSANN),” in *International Conference on Robotics and Automation*. IEEE, 2016.
- [14] C. E. Rasmussen and C. K. I. Williams, *Gaussian Processes for Machine Learning*. Mit Press, Jan. 2006.
- [15] S. M. M. De Rossi, N. Vitiello, T. Lenzi, R. Ronsse, B. Koopman, A. Persichetti, F. Vecchi, A. J. Ijspeert, H. van Der Kooij, and M. C. Carrozza, “Sensing Pressure Distribution on a Lower-Limb Exoskeleton Physical Human-Machine Interface,” *Sensors*, vol. 11, no. 1, pp. 207–227, Jan. 2011.
- [16] Wensing, Patrick M. Wang, Albert, Seok, Sangok, Otten, David, Lang, Jeffrey, and Kim, Sangbae, “Proprioceptive Actuator Design in the MIT Cheetah: Impact Mitigation and High-Bandwidth Physical Interaction for Dynamic Legged Robots,” *IEEE Transactions on Robotics*, vol. 33, no. 3, pp. 509–522, 2017.
- [17] J. Ramos, B. Katz, M. Y. M. Chuah, and S. Kim, “Facilitating Model-Based Control Through Software-Hardware Co-Design,” in *International Conference on Robotics and Automation*. IEEE, May 2018, pp. 566–572.
- [18] J. Ramos and S. Kim, “Humanoid dynamic synchronization through whole-body bilateral feedback teleoperation,” *IEEE Transactions on Robotics*, vol. 34, no. 4, pp. 953–965, Aug 2018.
- [19] M. Y. M. Chuah, “Design principles of multi-axis, large magnitude force sensors based on stress fields for use in human and robotic locomotion,” Ph.D. dissertation, Massachusetts Institute of Technology, 2018.